

# Vapor–Liquid Equilibria in the Low-Temperature Fischer–Tropsch Synthesis

Carlo Giorgio Visconti\*

Dipartimento di Energia, Politecnico di Milano, Piazza Leonardo da Vinci 32, 20133 Milano, Italy

## 1. INTRODUCTION

Fischer–Tropsch synthesis (FTS) is a surface-catalyzed polymerization process which converts synthesis gas ( $\text{CO} + \text{H}_2$ ) into syncrude, a mixture of primarily *n*-hydrocarbons with a broad range of chain length, rejecting oxygen as water or carbon dioxide. It is the preferred route for the production of specialty chemicals (base oils, *n*-paraffins, naphtha) and clean transportation fuels (gasoil, kerosene) from natural gas, coal, and biomass. Process selectivity can be controlled, within limits, both by selecting the proper catalyst formulation (active phase, promoters, support) and by tuning the process conditions (temperature, pressure,  $\text{H}_2/\text{CO}$ /inert species relative content).

Despite the low sulfur tolerance<sup>1,2</sup> and the higher cost compared to iron-based catalysts, which were responsible for most of the global syncrude production before the commissioning of Shell Pearl GTL plant in 2011,<sup>3</sup> cobalt-based catalysts are particularly attractive for three main reasons. Cobalt surface atoms show high intrinsic activity in the FTS: this allows operation at low temperature ( $<250\text{ }^\circ\text{C}$  and often even  $<230\text{ }^\circ\text{C}$ ), where methane selectivity is minimized and  $\text{C}_{5+}$  selectivity is maximized. Also, the adoption of cobalt brings about the predominant removal of oxygen atoms in  $\text{CO}$  coreactant as  $\text{H}_2\text{O}$  (the carbon selectivity to  $\text{CO}_2$  is below 1 mol %), as a consequence of the absence of a water gas shift activity (which is instead present on Fe-based FTS catalysts): this minimizes the consumption of carbon in oxygen rejection steps and leads to high thermal and carbon efficiencies.<sup>4</sup> Furthermore, this makes cobalt catalysts highly suited for natural gas derived syngas with a  $\text{H}_2/\text{CO}$  around 2, which satisfies the stoichiometry of the FTS. Third, the higher cost of cobalt is offset by the longer catalyst lifetime and the subsequent recovery of cobalt from the spent catalyst.<sup>4</sup> Hence, most of the industrial plants started-up in the last 20 years are based on promoted cobalt catalysts.

When operated at temperature below  $250\text{ }^\circ\text{C}$  (low-temperature Fischer–Tropsch, LTFT), the reaction products of cobalt-based (but also iron-based) catalysts are partially

vapor and partially liquid: accordingly, three-phase catalytic reactors are employed both at the lab-scale and at the industrial scale. In trickle-bed multitubular reactors with external cooling (such as the Shell HPS technology<sup>5</sup>) the solid phase (the heterogeneous catalyst) is present as a fixed bed within thin tubes (around 1 in. i.d.), the gaseous reactants are fed from the top and the biphasic products are formed progressively along the reactor axial coordinate. In slurry bubble column reactors (such as the Sasol SSBP technology<sup>6</sup>), the solid catalyst is suspended in the liquid products, and the reactants are fed from the bottom through a gas distributor: the gaseous products leave the reactor from the top, while the excess liquid phase is continuously extracted from the reactor after the separation from the powdered catalyst by filtration. The presence of a liquid phase covering the catalyst pellets and filling the catalyst pores may strongly affect the reactor performances: external mass transfer limitations may occur especially in the case of slurry bubble column reactors, while internal mass transfer restrictions may limit operations of packed bed reactors. In the case of slurry reactors, in addition, the hydrodynamics is strongly dependent on the liquid composition.<sup>7</sup>

Because of the strong exothermicity of the FTS ( $\Delta H^{\text{OR}} = -167\text{ kJ/mol}_{\text{CO}}$ ) and the high sensitivity to temperature of the process selectivity, the reaction heat has to be effectively removed from the reaction environment.<sup>8,9</sup> Multitubular reactors are designed as shell-and-tube type heat exchangers, in which the tubes in the bundle are filled with the catalyst pellets and are immersed in boiling water, which enables heat removal. Nevertheless, to maintain a satisfactory temperature control in the catalyst bed, the maximum diameter of the tubes

**Received:** May 16, 2013

**Revised:** July 5, 2013

**Accepted:** July 9, 2013

**Published:** July 9, 2013

is limited. Also, catalytic pellets with a nonuniform active phase distribution (such as egg-shell pellets) may be used to moderate the heat release, preventing at the same time the occurrence of strong intraporous mass transfer limitations.<sup>10</sup> This is often not enough, and in order to gain high values of the overall heat transfer coefficient, liquid waxes are recycled back to the reactor inlet so to operate the reactor as trickle bed with high liquid content.<sup>3</sup> A high gas recycle ratio may also be adopted, even though such a solution is usually less effective and more costly.<sup>3</sup> Alternative solutions have been proposed, such as the adoption of multitubular reactors loaded with highly conductive honeycomb monoliths.<sup>8,9,11</sup> In the case of slurry bed reactors, on the contrary, reaction heat is removed with high efficiency by heat exchangers immersed in the slurry bed, and the reactor is kept isothermal by the mixed liquid phase.

It is thus clear that the performances of LTFT catalysts and reactors are strongly related to and affected by the presence of a liquid phase. The same is true for the innovative LTFT reactor technologies proposed in the last years by both industrial and academic scientists, such as microchannel reactors,<sup>12,13</sup> monolith loop reactors,<sup>14,15</sup> foam-based reactors,<sup>16</sup> micro-fibrous entrapped catalyst (MFEC)-based reactors<sup>17</sup>, and highly conductive honeycomb-based<sup>9</sup> reactors. With this in the mind, Visconti and Mascellaro<sup>18</sup> have recently reported the development of a mathematical model able to predict, at the same time, the amount and the composition of liquid products formed in the low-temperature Fischer–Tropsch synthesis over a representative cobalt-based catalyst operating at process conditions typical of industrial operations. To achieve this goal, starting from a complete set of steady-state FTS runs carried out in a lab-scale reactor loaded with a 20 wt % Co/Al<sub>2</sub>O<sub>3</sub> catalyst, Visconti and Mascellaro<sup>18</sup> have developed a CO conversion kinetics model and a product distribution model, and they have combined the two models to be able to estimate the product yields in the reactor as a function of the process conditions. Yields have been finally used as input for an isothermal and isobaric vapor–liquid equilibrium (VLE) calculation.

This approach has a number of shortcomings. First of all, as pointed out in Visconti et al.,<sup>19</sup> the separate development of a rate expression for reactants conversion and a product distribution model is theoretically justified only if it can be assumed that the reaction products do not affect or participate in the monomer formation mechanism, and this is not likely to occur in the FTS. Often, in addition, both the CO conversion and the product distribution models are empirical, and this constrains the safe applicability of the resulting model only to the range of process conditions where the experimental data used to develop the models have been collected; no extrapolation is safe. Third, product distribution models often grant only a rough fitting of the experimental product distribution. For example, most of these models, including the ideal Anderson–Schulz–Flory model used in the work by Visconti and Mascellaro,<sup>18</sup> cannot account for the typical anomalies of the actual product distribution, that is the high methane selectivity, the low selectivity to C<sub>2</sub> species, and the change of slope of the Schulz–Flory distribution for a carbon number around 10. Also, these models do not distinguish between paraffins and olefins, but can only predict the distribution of lumped species with *n* carbon atoms.

On the basis of these considerations, a more fundamental approach is reported in this paper. Instead of using a CO conversion kinetics and a product distribution model to

quantify the product yields in the reactor, a detailed mechanistic kinetic model,<sup>20</sup> able to describe the rate of all the reaction steps involved in the FTS in the range of conditions of industrial interest ( $T = 210\text{--}235\text{ }^{\circ}\text{C}$ ,  $P = 8\text{--}25$  bar, H<sub>2</sub>/CO inlet molar ratio = 1.8–2.7, GHSV = 2000–7000 cm<sup>3</sup> (STP) h<sup>-1</sup> g<sup>-1</sup>), has been used to describe the product yields in the reactor as a function of the process conditions. Calculated product yields have been then used as input for a nonideal isothermal and isobaric vapor–liquid equilibrium calculation. This has allowed a precise estimation of the yield and the VLE of H<sub>2</sub>O and of each of the produced *n*-paraffins and linear  $\alpha$ -olefins upon changing the process conditions.

## 2. MODELING SECTION

**2.1. Detailed Kinetic Model.** The approach adopted to develop the detailed kinetic model is the following. Mostly based on the analysis of the literature data concerning the FTS reaction pathways, first a detailed FTS mechanism for a cobalt-based catalyst has been defined, explaining the consumption of the reactants and the synthesis of each reaction product through the evolution of adsorbed reaction intermediates. Then, equilibrium constants or elementary rate laws have been attributed to each reaction step, and the resulting kinetic scheme has been fitted to a comprehensive set of FTS data collected in the range of process conditions typical of industrial operations. In light of the small quantities involved (carbon selectivity below 5 mol %), all the oxygenated products different from H<sub>2</sub>O have been ignored. More details on the adopted approach can be found elsewhere.<sup>20</sup>

The H-assisted CO dissociation mechanism<sup>21,22</sup> has been used to describe the CO activation process. According to this mechanism, H<sub>2</sub> chemisorbs on two adjacent free catalytic sites in the dissociated state, while CO is first chemisorbed reversibly in the molecular state. It is then hydrogenated two times giving the formyl intermediate (HCO<sub>ads</sub>) after the first H-addition and the hydroxymethylene species (HCOH<sub>ads</sub>) after the second hydrogenation. The alkyl mechanism, with CH<sub>2ads</sub> as chain growth monomer, has been used to describe the chain growth process. Accordingly, hydroxymethylene dissociates into CH<sub>ads</sub> and OH<sub>ads</sub>, that in turn react with two adsorbed hydrogen atoms forming the polymerization monomer (CH<sub>2ads</sub>) and H<sub>2</sub>O, respectively. The monomer can add an H<sub>ads</sub> species, forming the initiator required for the chain growth (methyl species) or can attack a growing chain being inserted into the active site-alkyl bond. Termination of the polymerization process is the result of two alternative routes, involving either the addition or the rejection of an H<sub>ads</sub>: the addition of an adsorbed hydrogen atom to the growing intermediates results in the formation of a *n*-paraffin, while the  $\beta$ -hydride elimination from the growing intermediates results in the synthesis of a linear  $\alpha$ -olefin.

Details on the rate law attributed to each reaction step, as well as details on the approach followed to estimate the 13 adaptive parameters involved in the detailed kinetic model, are given elsewhere.<sup>20</sup> It should be noted, however, that both the mechanistic CO consumption rate expression used in Visconti and Mascellaro,<sup>18</sup> and the detailed kinetic model herein implemented, have been developed under the same assumptions on the dominant reaction pathway as well as on the rate determining step (RDS) in the CO activation mechanism. In both the cases, in fact, the H-assisted CO activation mechanism has been adopted to describe the formation of the chain growth monomer, and the formyl hydrogenation has been found to be

the RDS, with  $\text{CO}_{\text{ads}}$  and  $\text{HCO}_{\text{ads}}$  as the most abundant reaction intermediates (MARIs). This is in full agreement with what has been recently shown by the research groups of Iglesia and Mavrikakis<sup>21</sup> through experimental data and DFT calculations, respectively.

It is worth noting that experimental data used in ref 20 to estimate the kinetic parameters differ from those adopted by Visconti and Mascellaro.<sup>18</sup> Data adopted in ref 20 were collected with an impregnated 15 wt %  $\text{Co}/\text{Al}_2\text{O}_3$  catalyst in the following ranges of process conditions:  $P = 8\text{--}25$  bar,  $T = 210\text{--}235$  °C,  $\text{H}_2/\text{CO}$  feed ratio =  $1.8\text{--}2.7$  mol mol<sup>-1</sup>,  $\text{GHSV} = 2000\text{--}7000$  cm<sup>3</sup> (STP) h<sup>-1</sup> g<sub>cat</sub><sup>-1</sup>, Ar = 2.5 mol %. Within these intervals the CO conversion varied from 12 and 42%, with a  $\text{CH}_4$  and  $\text{C}_{5+}$  carbon selectivities in the ranges 8–12% and 20–34%, respectively. The catalyst modeled in ref 18 instead, had a cobalt loading of 20 wt % and was tested at temperatures between 220 and 230 °C, a  $\text{H}_2/\text{CO}$  feed ratio between 1.40 and 2.15 mol mol<sup>-1</sup>,  $\text{GHSV} = 5400\text{--}7400$  cm<sup>3</sup> (STP) h<sup>-1</sup> g<sub>cat</sub><sup>-1</sup>, in the presence of 23.5–45.1 mol % of  $\text{N}_2$  in the feed. Accordingly, a direct comparison between the performances of the product yields and vapor–liquid repartition model proposed in ref 18 and the performances of the model herein developed will not be possible. Nevertheless, at the investigated process conditions the performances of the two catalysts were quite similar in terms of CO conversion (between 20 and 40%) as well as in terms of chain growth probability (around 0.89).

**2.2. Vapor–Liquid Equilibrium.** The vapor–liquid equilibrium of each species present in the reacting mixture was computed by imposing the equivalence between the fugacities of the  $i$ -species in the liquid phase  $\hat{f}_i^L$  and in the vapor phase  $\hat{f}_i^V$ , eq 1:

$$\hat{f}_i^L(T, P, \underline{x}) = \hat{f}_i^V(T, P, \underline{y}) \quad (1)$$

In eq 1  $T$  and  $P$  are the system temperature and pressure,  $\underline{x}$  is the array of the molar fractions in the liquid phase, and  $\underline{y}$  is the array of the molar fractions in the vapor phase. The  $\hat{\phi}^L/\hat{\phi}^V$  (or symmetric) approach, explicating the vapor and liquid phase fugacities as shown in eq 2, has been used to calculate the two terms of eq 1:

$$x_i \hat{\phi}_i^L(T, P, \underline{x}) = y_i \hat{\phi}_i^V(T, P, \underline{y}) \quad (2)$$

In eq 2,  $x_i$  is the molar fraction of the  $i$ -species in the liquid phase,  $y_i$  is its molar fraction in the vapor phase,  $\hat{\phi}_i^L(T, P, \underline{x})$  is the fugacity coefficient of the  $i$ -species in the liquid mixture at the system temperature, pressure, and composition, and  $\hat{\phi}_i^V(T, P, \underline{y})$  the fugacity coefficient in the vapor phase of the same species at the same process conditions. Following an approach similar to those adopted by Fox and Tam,<sup>23</sup> Marano and Holder,<sup>24</sup> and Derevich et al.,<sup>25</sup> both the liquid phase and vapor phase fugacity coefficients were calculated through the Peng–Robinson (PR) equation of state (EOS). The van der Waals mixing rules with one binary interaction parameter were used to estimate the attractive parameter and the covolume involved in the EOS. The acentric factors and the binary interaction parameters were taken from a proprietary data-bank.

Once the product yield of the  $i$ -species ( $F_i$ ) was computed through the detailed kinetic model described in section 2.1, in order to find its vapor/liquid split, eq 2 was solved coupled with the material balance 3:

$$F_i = V \cdot y_i + L \cdot x_i \quad (3)$$

$V$  and  $L$  in eq 3 are the molar flow rates of the vapor and liquid phases, respectively.

The VLE has been computed for  $\text{CO}$ ,  $\text{H}_2$ ,  $\text{H}_2\text{O}$ , Ar, the  $\text{C}_1\text{--}\text{C}_{30}$   $n$ -paraffins, the  $\text{C}_2\text{--}\text{C}_{30}$  linear  $\alpha$ -olefins, and for the  $n\text{-C}_{36}\text{H}_{74}$  species. The latter has been used as a lump of the  $\text{C}_{31+}$  hydrocarbons, which have not been singularly considered in the VLE calculations because the critical temperature and pressure for most of these components, necessary to solve the phase equilibria, are not available in the literature. This simplification differs from that adopted in the model proposed by Visconti and Mascellaro,<sup>18</sup> where all the species with more than 30 carbon atoms, representing less than the 1 mol % of the total hydrocarbon products formed in the LTFT at typical process conditions, were neglected, and it is expected to further improve the quality of the results. Also the distinction between paraffins and olefins was not considered by the model by Visconti and Mascellaro,<sup>18</sup> which on the basis of a single chain growth parameter, was only able to describe the integral sum of the paraffin and the olefin yields with  $n$  carbon atoms (assumed as  $n$ -paraffin in VLE calculations).

### 3. RESULTS AND DISCUSSION

**3.1. Product Yields.** In Figure 1a, a typical fitting of the experimental product distribution with the detailed kinetic

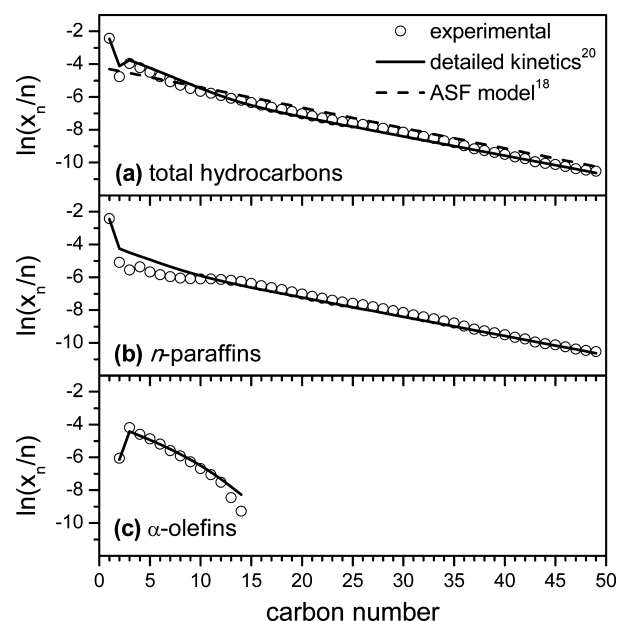


**Figure 1.** (a) Comparison among experimental, ideal (ASF), and calculated (detailed kinetic model) product distributions; comparison between experimental and calculated (detailed kinetic model) (b) paraffins and (c) olefins distributions. Process conditions: 230 °C, 20 bar, 2.1 mol $\text{H}_2$ /mol $\text{CO}$ , 5000 cm<sup>3</sup><sub>syngas</sub> (STP) h<sup>-1</sup> g<sub>cat</sub><sup>-1</sup>, 2.5 mol% Ar in the feed.

model developed in ref 20 is shown. The product distribution estimated through the ideal Anderson–Schulz–Flory (ASF) model used by Visconti and Mascellaro<sup>18</sup> is also shown for comparison purposes. Differently from the ideal ASF model, the detailed kinetic model more accurately describes the experimental data, accounting also for the characteristic features of the experimental Schulz–Flory product distribution, namely the high methane selectivity, the low selectivity to ethylene and the change of slope with growing carbon number. Also, such model is able to discriminate between  $n$ -paraffins and linear  $\alpha$ -

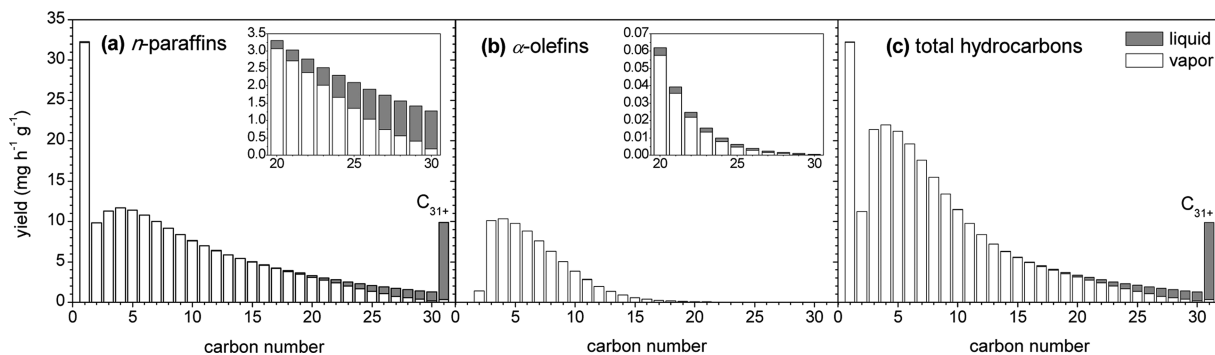


**Figure 2.** Liquid and vapor mass flows of each one of the reaction products: (a) paraffins, (b) olefins, (c) total hydrocarbons. Process conditions as in Figure 1.

olefins: a typical comparison between the experimental and the calculated product distribution is shown in Figure 1b,c.

It is worth noting that the better fit of the experimental data granted by the detailed kinetic model herein adopted is obtained by adding only one extra adaptive parameter with respect to the combined CO conversion and product distribution models developed in ref 18. In the product yields model developed in ref 18, 12 adaptive parameters were used (4 parameters for the CO conversion kinetics and 8 for the single chain growth probability product distribution model), while 13 parameters were used for the detailed kinetic model developed in ref 20 and used herein.

**3.2. Vapor–Liquid Equilibrium.** The product yields calculated through the detailed kinetic model have been used as input for the multicomponent isothermal and isobaric flash calculation to compute the VLE of each species contained in the reacting mixture. At all simulated process conditions, CO, H<sub>2</sub>, N<sub>2</sub>, and H<sub>2</sub>O were found to be completely in the vapor phase. The same is true for the lightest reaction products. In Figure 2, as an example, the liquid and vapor mass flows of each one of the products formed at typical LTFT process conditions are shown. Figure 2a refers to *n*-paraffins, Figure 2b refers to linear  $\alpha$ -olefins, and Figure 2c refers to total hydrocarbons. The resulting vapor and liquid hydrocarbon breakdowns in the vapor and liquid stream are shown in Figure 3a (where the estimated compositions of vapor and liquid phases at the reactor outlet are plotted), while the Schulz–Flory plots of the total vapor and liquid hydrocarbon distributions at the reactor outlet are shown in Figure 3b.

Essentially, the hydrocarbons with less than 20 carbon atoms are almost entirely vapor at the adopted process conditions (i.e.,  $L_i/(L_i + V_i) < 5\%$ ), while the C<sub>31+</sub> species are almost entirely liquid ( $L_i/(L_i + V_i) > 95\%$ ). The species with a number of carbon atoms between 20 and 30, on the contrary, are split between the two phases. Vapor is dominant (i.e.,  $V_i/(L_i + V_i) > 50\%$ ) for C<sub>20</sub>–C<sub>26</sub> species, liquid is dominant for C<sub>27</sub>–C<sub>30</sub> species: the carbon number crossover prediction is 27. Insets of Figure 2 panels a and b reveal that each olefin is slightly more volatile than the corresponding paraffin: even the longest olefin we included in the model, the 1-triacontene (C<sub>30</sub>H<sub>60</sub>), is predominantly in the vapor phase, while the paraffins with 27 or more carbon atoms are mostly liquid.

Among the vapor species, that with the highest yield at the conditions simulated in Figure 2 is CH<sub>4</sub>, which is well-known to be the most abundant (and usually undesired) hydrocarbon product of the Fischer–Tropsch synthesis. Among the liquid species, on the other hand, the most abundant hydrocarbon is

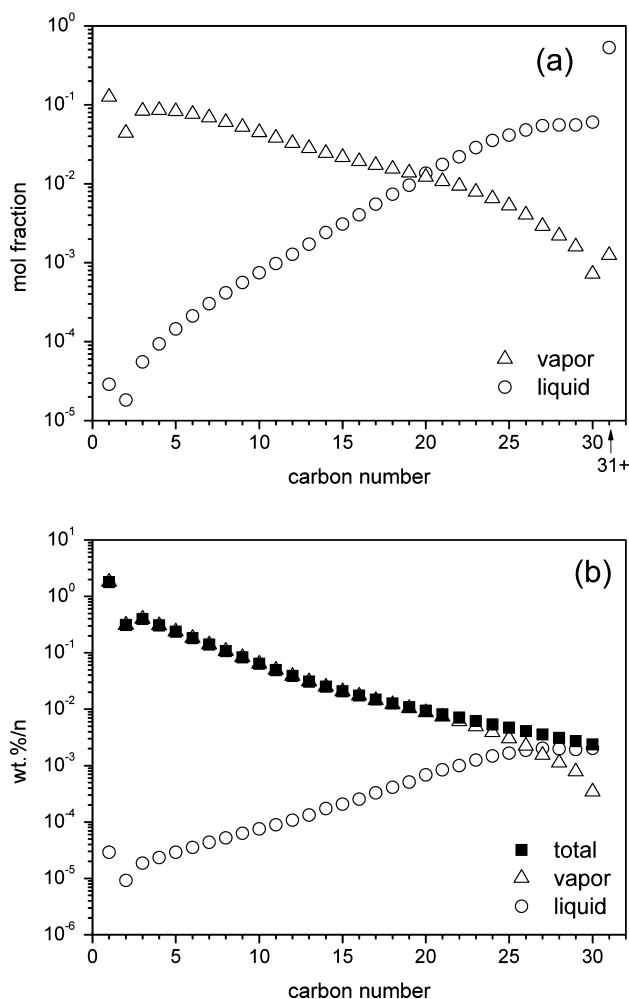


**Figure 3.** (a) Estimated vapor and liquid compositions at the reactor outlet; (b) Schulz–Flory plot of the total vapor and liquid hydrocarbon distributions at the reactor outlet. Process conditions as in Figure 1.

the C<sub>31+</sub> lumped species, whose condensed fraction represents almost 97% of the total amount formed in the reactor. The hydrocarbon vaporization ratio, defined as the molar ratio between the vapor and the liquid flow rates, is around 106, which means that more than 99.1 mol % of the hydrocarbon products are in the vapor phase at these conditions. The total vaporization ratio, evaluated by including CO, H<sub>2</sub>, and H<sub>2</sub>O in the calculation, is instead more than 4000, which means that

**Table 1. Set of Hypotheses Adopted to Perform VLE Calculations**

series name tag	product yields model	hydrocarbons considered in the VLE	distinction between paraffins and olefins	ref
Visconti&Mascellaro	CO conversion kinetics + ASF product distribution	C <sub>1</sub> –C <sub>30</sub>	no	18
det kin	detailed kinetics	C <sub>1</sub> –C <sub>30</sub>	no	this work
det kin olef	detailed kinetics	C <sub>1</sub> –C <sub>30</sub>	yes	this work
this paper	detailed kinetics	C <sub>1</sub> –C <sub>30</sub> + C <sub>36</sub> H <sub>74</sub> (lumped species)	yes	this work

more than 99.97 mol % of the molecules flowing in the reactor are vaporized. This result confirms the indication reported in the literature by Philippe et al.,<sup>26</sup> who claim, on the basis of thermodynamic equilibrium calculation, that under typical low-temperature FTS condition (20 bar, 230 °C) more than 99 mol % of the reacting species are in the gaseous phase.

It is interesting to compare the result of this calculation with those reported by Visconti and Mascellaro.<sup>18</sup> In that case, simulating a similar Co-based FT catalyst working at similar process conditions (the main difference, the pressure (25 bar<sup>18</sup> vs 20 bar<sup>this work</sup>), is compensated by a different inert content in the feed (23.5%<sup>18</sup> vs 2.5%<sup>this work</sup>) and similar CO conversion (around 30%), it has been found that (i) C<sub>1</sub>–C<sub>9</sub> species are almost entirely vapor; (ii) C<sub>10</sub>–C<sub>30</sub> species are split into a vapor fraction, prevalent for the C<sub>10</sub>–C<sub>22</sub> species, and a liquid fraction, prevalent for the C<sub>23</sub>–C<sub>30</sub> species; (iii) the most abundant species in the vapor phase are C<sub>8</sub> hydrocarbons (which according to the ideal ASF distribution adopted in the paper is also the most abundant hydrocarbon product in the reactor); (iv) the most abundant species in the liquid phase are C<sub>27</sub> hydrocarbons; (v) more than 95 mol % of the C<sub>1</sub>–C<sub>30</sub> hydrocarbons are in the vapor phase; (vi) the fraction of reacting mixtures in the vapor phase, is higher than 99.9 mol %. The observed variances, which do not change the message on the extremely high vaporization ratio in the reactor, can be explained considering the differences between the model here proposed and the model by Visconti and Mascellaro,<sup>18</sup> namely, (i) the description of the product yields through a detailed kinetic model instead of the ideal ASF distribution, resulting in a more reliable product distribution; (ii) the introduction of the species C<sub>36</sub>H<sub>74</sub> as a lump of the C<sub>31+</sub> products; (iii) the removal of the hypothesis that all the products are paraffins, and the introduction of a distinction between paraffinic and olefinic products.

To better clarify the effects of the hypotheses (i–iii), a set of simulations has been carried out, where one hypothesis per time has been introduced starting from the model used in the paper by Visconti and Mascellaro<sup>18</sup> (Table 1).

In Figure 4, the results of the VLE performed by following the approach proposed in ref 18 is shown (curve “Visconti&Mascellaro”) in terms of liquid fraction  $L_i/(L_i + V_i)$ : at 230 °C, 20 bar, 2.1 mol<sub>H<sub>2</sub></sub><sup>in</sup>/mol<sub>CO</sub><sup>in</sup> and CO conversion around 30%, C<sub>17+</sub> species are in the condensed state for more than 5%, C<sub>24+</sub> for more than 50%, and C<sub>28+</sub> for more than 80%. What happens if we replace the empirical product yields model proposed in ref 18 with the detailed kinetic model, without introducing the lumped species C<sub>36</sub>H<sub>74</sub> and without distinguishing between paraffins and olefins (Figure 4, curve “det kin”)? The vaporization ratio of the heaviest species dramatically decreases: only C<sub>24+</sub> hydrocarbons are in the condensed state for more than 5% and only the C<sub>30</sub> hydrocarbons are more liquid than vapor (53% vs 47%). Such a strong effect can be explained considering that the ideal ASF model, used in ref 18

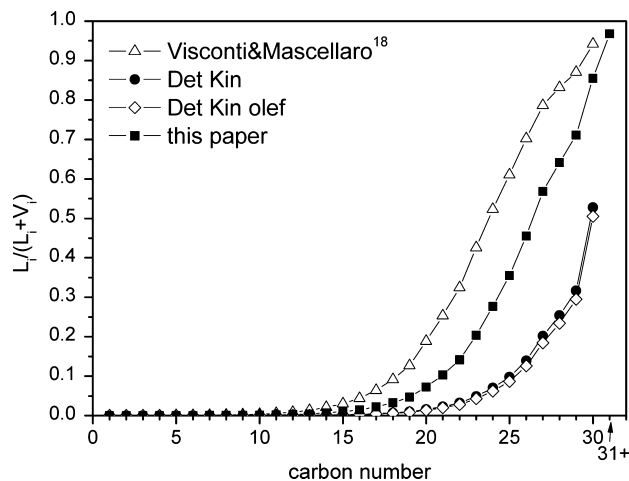


**Figure 4.** Results of the VLE calculation performed under different sets of simplifying hypotheses. Legends refer to Table 1. Process conditions as in Figure 1.

to compute the product yields in the reactor, overestimates the heaviest products (cf. Figure 1), while the detailed kinetics used in this paper accurately describes the experimental product distribution: the higher amount of heavy species favors in fact their liquefaction.

Slight effects are instead associated to the distinction between paraffins and olefins: the curves “det kin” and “det kin olef” shown in Figure 4 show indeed only minor deviations.

The dramatic increase of the vaporization ratio resulting from the adoption of the detailed kinetic model is partially compensated by the introduction of C<sub>36</sub>H<sub>74</sub> as a lumped species. The curve “this paper” shown in Figure 4 is in fact intermediate between that of Visconti&Mascellaro<sup>18</sup> and those obtained with the model herein proposed without considering the C<sub>31+</sub> species: C<sub>20+</sub> species are more than 5% in the condensed state, C<sub>27+</sub> more than 50%, and C<sub>30+</sub> more than 80%. Such an effect can be explained considering that because of the binary interactions between the hydrocarbons, the addition of the lumped species, which is primarily in the liquid phase, favors the condensation of all the other hydrocarbons, even though it represents only a minor fraction (3.6 wt %) of the hydrocarbon product pool.

The effects of the process conditions on the VLE are shown in Figure 5 in terms of vapor fraction ( $V_i/(L_i + V_i)$ ). Interestingly, in the narrow range of process conditions investigated, the effects of the process conditions on the VLE are minor, except in the case of pressure (Figure 5b). Upon decreasing the pressure, in fact, the vaporization strongly increases, so that at 8 bar all the products are vaporized. This can be explained considering the pressure effects both on the product distribution and on the VLE. As it has been shown in ref 18, indeed, the product distribution is shifted toward low

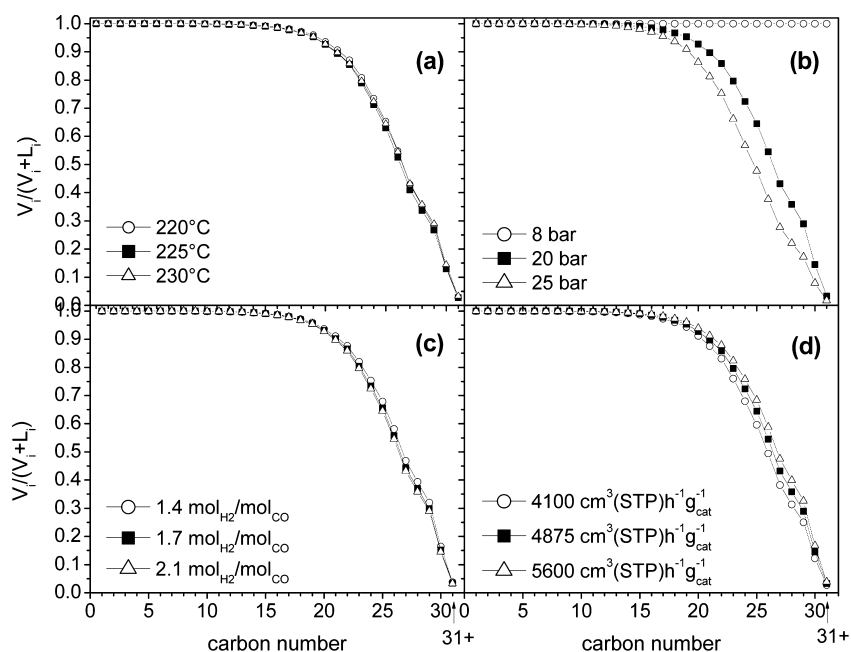


**Figure 5.** Effects of the process conditions on the VLE: (a) temperature, (b) pressure, (c)  $H_2/CO$  inlet ratio, (d) GHSV. Other process conditions as in Figure 1.

molecular weight hydrocarbons at low pressure: the predicted carbon selectivity to  $C_{5+}$  products, for example, is around 75% at 20 bar and around 57% at 8 bar. Accordingly, the amount of species able to condensate at these process conditions is drastically decreased. The pressure effect on the VLE further enhances such a trend: upon decreasing the pressure, in fact, phase equilibria move to the vapor species.

To decouple the pressure effects on the product distribution and on the product repartition in a vapor and in a liquid phase, simulations have been performed where vapor–liquid equilibria have been computed at different pressures for the same mixture. As a “reference mixture”, that obtained at 20 bar was selected. The vaporization ratio curves of such a mixture obtained at 8, 20, and 25 bar are shown in Figure 6. As expected, observed effects are still important, but much less evident than those shown in Figure 5b. This is particularly evident at 8 bar: while the products obtained at this condition are completely vaporized (Figure 5b), the hydrocarbon

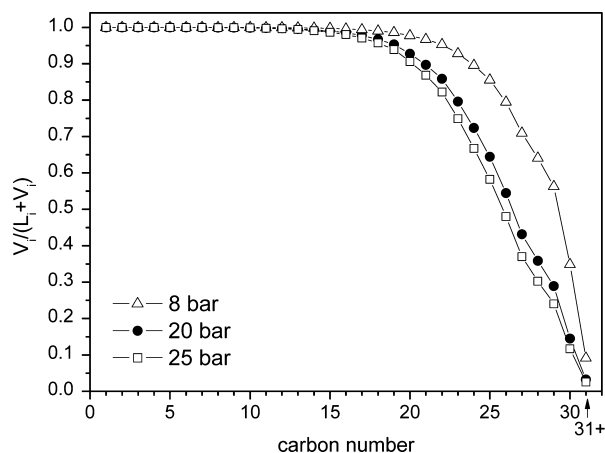


**Figure 6.** Vaporization ratio curves obtained at different pressures. Other process conditions as in Figure 1.

products formed at 20 bar and flashed at 8 bar are only partially vaporized (Figure 6). This means that the effects of pressure on the product distribution do affect the VLE much more than what the pressure itself does on the equilibria.

The strong effects of pressure on the reactor performances are particularly interesting in light of the recent industrial trend to increase the process pressure both to decrease the equipment size and to compensate the high inert content in the process loop. This is the case of each of the 24 Shell HPS multitubular reactors at the Ras Laffan (Qatar) site,<sup>3</sup> which operate at a total pressure of 60 bar, with a low CO per pass conversion and a consequent high recycle ratio so to limit the process duty and to boost the overall heat transfer coefficient.<sup>3</sup> The increase of pressure may indeed have relevant consequences on both the products distribution and the vapor–liquid equilibria, thus resulting in an unconventional reaction environment (probably characterized by an increased content of liquids) whose effects on the catalyst performances and lifetime, difficult to be predicted, merit an in depth analysis.

#### 4. CONCLUSION

Vapor–liquid equilibria within low-temperature Fischer–Tropsch reactors have been simulated in this paper through the combined application of a detailed kinetic model and a nonideal isothermal and isobaric phase equilibria. The formation of a liquid phase in the low-temperature Fischer–Tropsch synthesis reactors may be predicted, and its composition and quantity can be accurately calculated.

At the typical process conditions, more than 99 mol % of the hydrocarbon products are in the vapor phase, which implies that more than 99.9 mol % of the reacting mixture is vaporized. In the narrow range of conditions of industrial interest, process variables have been found to have only minor effects on the VLE. In this regards, the most relevant process variable has been found to be the pressure, which affects both the products distribution and the vapor–liquid split.

The VLE model herein proposed is superior with respect to those available in the open literature, which are based on a number of simplifying assumptions which are often not valid, such as the adoption of the ideal ASF model to describe the hydrocarbon product distribution,<sup>7,18,24</sup> the use of paraffins as unique reaction products,<sup>7,18</sup> the use of pseudocomponents to limit the computational burden,<sup>24,27</sup> or the adoption of the Raoult's law to describe phase equilibria.<sup>7,28,29</sup> It has been shown indeed that any inaccuracy in the prediction of the product distribution may have relevant effects on the phase equilibria calculations.

Moreover, the model herein proposed is the only one able to describe, on the basis of a comprehensive kinetic model, both the VLE and the product yields as a function of the process conditions. Other similar models available in the literature,<sup>27,30</sup> indeed, combine a rate expression for reactants conversion and a product distribution model to describe the product yields, even though this is not theoretically justified when, as in this case, the reaction products do affect the monomer formation mechanism.<sup>19</sup>

Calculations of this type are of the utmost importance, not only in slurry reactors where the hydrodynamics and the presence of mass-transfer restrictions depend strongly on liquid composition, but also in the design, operation, and analysis of conventional and innovative fixed-bed reactors,<sup>31</sup> where the presence of a liquid phase trickling down the tubes may affect the mass and heat transfer performances, as well as the pressure drops.

## AUTHOR INFORMATION

### Corresponding Author

\*E-mail: carlo.visconti@polimi.it. Tel.: 0039 02 2399 3297. Fax: 0039 02 2399 3318.

### Notes

The authors declare no competing financial interest.

## ACKNOWLEDGMENTS

Dr. Marina Mascellaro is gratefully acknowledged for her support with the VLE calculations.

## NOTATION

- $\hat{f}_i$  = fugacities of the  $i$ -species in a mixture (bar)  
 $F_i$  = yield of the  $i$ -species (liquid + vapor) (mol/s)  
 $L$  = liquid molar flow rate (mol/s)  
 $P$  = pressure (bar)  
 $T$  = temperature (K)  
 $V$  = vapor molar flow rate (mol/s)  
 $\underline{x}$  = array of the components molar fractions in the liquid phase (–)  
 $x_i$  = molar fraction of the  $i$ -species in the liquid phase (–)  
 $\underline{y}$  = array of the components molar fractions in the vapor phase (–)  
 $y_i$  = molar fraction of the  $i$ -species in the vapor phase (–)

### Greek Letters

- $\Delta H^{\text{OR}}$  = standard heat of reaction (kJ/mol)  
 $\hat{\phi}_i$  = fugacity coefficient of the  $i$ -species in a mixture (–)

### Subscripts and Superscripts

- ads adsorbed species  
 $i$   $i$ -species  
 $L$  liquid phase  
 $V$  vapor phase

## Abbreviations

- ASF = Anderson-Schulz-Flory  
DFT = density functional theory  
EOS = equation of state  
FTS = Fischer–Tropsch synthesis  
GTL = gas to liquids  
HPS = heavy paraffin synthesis  
i.d. = internal diameter  
LTFT = low-temperature Fischer–Tropsch  
MARI = most abundant reaction intermediate  
PR = Peng–Robinson  
RDS = rate determining step  
STP = standard temperature and pressure  
SSBP = Sasol slurry bed process  
VLE = vapor liquid equilibrium

## REFERENCES

- Visconti, C. G.; Lietti, L.; Forzatti, P.; Zennaro, R. Fischer–Tropsch synthesis on sulphur poisoned Co/Al<sub>2</sub>O<sub>3</sub> catalyst. *Appl. Catal. A: Gen.* **2007**, *330*, 49.
- Visconti, C. G.; Lietti, L.; Tronconi, E.; Forzatti, P.; Zennaro, R.; Rossini, S. Detailed kinetics of the Fischer–Tropsch synthesis over Co-based catalysts containing sulphur. *Catal. Today* **2010**, *154*, 202.
- de Klerk, A.; Li, Y.-W.; Zennaro, R. In *Greener Fischer–Tropsch Processes*; Maitlis, P. M., de Klerk, A., Eds.; Wiley-VCH: Weinheim, Germany, 2013; pp 53–80.
- Soled, S. L.; Iglesia, E.; Fiato, R. A.; Baumgartner, J. E.; Vroman, H.; Míseo, S. Control of metal dispersion and structure by changes in the solid-state chemistry of supported cobalt Fischer–Tropsch catalysts. *Top. Catal.* **2003**, *26*, 101.
- Eilers, J.; Posthuma, S. A.; Sie, S. T. The Shell middle distillate synthesis process (SMDS). *Catal. Lett.* **1991**, *7*, 253.
- Espinoza, R. L.; Steynberg, A. P.; Jager, B.; Vosloo, A. C. Low temperature Fischer–Tropsch synthesis from a Sasol perspective. *Appl. Catal. A: Gen.* **1999**, *186*, 13.
- Caldwell, L.; Van Vuuren, D. S. On the formation and composition of the liquid phase in Fischer–Tropsch reactors. *Chem. Eng. Sci.* **1986**, *41*, 89.
- Visconti, C. G.; Tronconi, E.; Groppi, G.; Lietti, L.; Iovane, M.; Rossini, S.; Zennaro, R. Monolithic catalysts with high thermal conductivity for the Fischer–Tropsch synthesis in tubular reactors. *Chem. Eng. J.* **2011**, *171*, 1294.
- Visconti, C. G.; Tronconi, E.; Lietti, L.; Groppi, G.; Forzatti, P.; Cristiani, C.; Zennaro, R.; Rossini, S. An experimental investigation of Fischer–Tropsch synthesis over washcoated metallic structured supports. *Appl. Catal. A: Gen.* **2009**, *370*, 93.
- Iglesia, E.; Soled, S. L.; Baumgartner, J. E.; Reyes, S. C. Synthesis and catalytic properties of eggshell cobalt catalysts for the Fischer–Tropsch synthesis. *J. Catal.* **1995**, *153*, 108.
- Visconti, C. G.; Groppi, G.; Tronconi, E. Accurate prediction of the effective radial conductivity of highly conductive honeycomb monoliths with square channels. *Chem. Eng. J.* **2013**, *223*, 224.
- Wang, Y.; Tonkovich, L.; Mazanec, T.; Daly, F. D.; VanderWiel, D.; Hu, J.; Cao, C.; Kibby, C.; Li, X. S.; Briscoe, M. D.; Gano, N.; Chin, Y. Fischer–Tropsch synthesis using microchannel technology and novel catalyst and microchannel reactor, US 7,084,180, 2006
- Bowe, M. J.; Lee-Tuffnell, C. D. Catalytic reactor and process, WO 2004050799, 2004
- de Deugd, R. M.; Chougule, R. B.; Kreutzer, M. T.; Meeuse, F. M.; Grievink, J.; Kapteijn, F.; Moulijn, J. A. Is a monolithic loop reactor a viable option for Fischer–Tropsch synthesis? *Chem. Eng. Sci.* **2003**, *58*, 583.
- Hilmen, A. M.; Bergene, E.; Lindvåg, A.; Schanke, D.; Eri, S.; Holmen, A. Fischer–Tropsch synthesis on monolithic catalysts with oil circulation. *Catal. Today* **2005**, *105*, 357.
- Lacroix, M.; Dreibine, L.; de Tymowski, B.; Vigneron, F.; Edouard, D.; Bégin, D.; Nguyen, P.; Pham, C.; Savin-Poncet, S.; Luck,

F.; Ledoux, M.-J.; Pham-Huu, C. Silicon carbide foam composite containing cobalt as a highly selective and re-usable Fischer–Tropsch synthesis catalyst. *Appl. Catal. A: Gen.* **2011**, *397*, 62.

(17) Sheng, M.; Yang, H.; Cahela, D. R.; Tatarchuk, B. J. Novel catalyst structures with enhanced heat transfer characteristics. *J. Catal.* **2011**, *281*, 254.

(18) Visconti, C. G.; Mascellaro, M. Calculating the products yield and their vapour–liquid equilibrium in the low-temperature Fischer–Tropsch synthesis. *Catal. Today* **2013**, *214*, 61–73.

(19) Visconti, C. G.; Tronconi, E.; Lietti, L.; Zennaro, R.; Forzatti, P. Development of a complete kinetic model for the Fischer–Tropsch synthesis over Co/Al<sub>2</sub>O<sub>3</sub> catalysts. *Chem. Eng. Sci.* **2007**, *62*, 5338.

(20) Visconti, C. G.; Tronconi, E.; Lietti, L.; Forzatti, P.; Rossini, S.; Zennaro, R. Detailed kinetics of the Fischer–Tropsch synthesis on cobalt catalysts based on H-assisted CO activation. *Top. Catal.* **2011**, *54*, 786.

(21) Ojeda, M.; Nabar, R.; Ishikawa, A. U.; Mavrikakis, M.; Iglesia, E. CO activation pathways and the mechanism of the Fischer–Tropsch synthesis. *J. Catal.* **2010**, *272*, 287.

(22) Storsæter, S.; Chen, D.; Holmen, A. Microkinetic modelling of the formation of C<sub>1</sub> and C<sub>2</sub> products in the Fischer–Tropsch synthesis over cobalt catalysts. *Surf. Sci.* **2006**, *600*, 2051.

(23) Fox, J. M.; Tam, S. S. Correlation of slurry reactor Fischer–Tropsch yield data. *Top. Catal.* **1995**, *2*, 285.

(24) Marano, J. J.; Holder, G. D. Characterization of Fischer–Tropsch liquids for vapor–liquid equilibria calculations. *Fluid Phase Equilib.* **1997**, *138*, 1.

(25) Derevich, I. V.; Ermolaev, V. S.; Mordkovich, V. Z. Liquid–vapor thermodynamic equilibrium in Fischer–Tropsch synthesis products. *Threor. Found. Chem. Eng.* **2008**, *42*, 216.

(26) Philippe, R.; Lacroix, M.; Dreibine, L.; Pham-Cuu, C.; Edouard, D.; Savin, S.; Luck, F.; Schweich, D. Effect of structure and thermal properties of a Fischer–Tropsch catalyst in a fixed bed. *Catal. Today* **2009**, *147S*, S305.

(27) Ahon, V. R.; Costa, E. F., Jr.; Monteagudo, J. E. P.; Fontes, C. E.; Biscaia, E. C., Jr.; Lage, P. L. C. A comprehensive mathematical model for the Fischer–Tropsch synthesis in well mixed slurry reactors. *Chem. Eng. Sci.* **2005**, *60*, 677.

(28) Raje, A. P.; Bavis, B. H. Effect of vapor–liquid equilibrium on Fischer–Tropsch hydrocarbon selectivity for a deactivating catalyst in slurry reactor. *Energy Fuels* **1996**, *10*, 552.

(29) Zhan, X.; Davis, B. H. Two-alpha Fischer–Tropsch product distribution. A role for vapor–liquid equilibrium? *Petrol. Sci. Technol.* **2000**, *18*, 1037.

(30) Yermakova, A.; Anikeev, V. I. Thermodynamic calculations in the modeling of multiphase processes and reactors. *Ind. Eng. Chem. Res.* **2000**, *39*, 1453.

(31) Visconti, C. G. A novel intensified modular reactor for the Fischer–Tropsch synthesis. *Chim. Oggi (Milestone in Chemistry Supplement)* **2011**, *29*, 9.